DISPERSION EFFECTS ON GRATING-ASSISTED OUTPUT COUPLERS UNDER ULTRAFAST PULSE EXCITATIONS

Tao Liang[1] and Richard W. Ziolkowski[1]
[1] Electromagnetics Laboratory
Department of Electrical and Computer Engineering
University of Arizona
Tucson, Arizona 85721-0104

Received 5 August 1997

ABSTRACT: *The effects of dispersion on the performance of finite-length grating-assisted output couplers driven by ultrafast pulses are studied. Two different FDTD formulations of Lorentz dispersion are treated, and both dispersive waveguides and grating teeth are considered. The impact of dispersion on the output beams is quantified. © 1998 John Wiley & Sons, Inc.* Microwave Opt Technol Lett 17: 17–23, 1998.

Key words: *FDTD modeling; grating-assisted coupler; dielectric waveguide; dispersion; ultrafast optical pulses*

1. INTRODUCTION

The interaction between electromagnetic waves and materials needs to be understood and characterized for the successful design of any device used for ultrafast pulse applications. Since material dispersion is the phenomenon which results from the change of material properties with the frequency content of the interacting electromagnetic waves, it is one of the most intrusive effects associated with ultrafast pulse applications. In this letter, we will investigate the effects of dispersion on the performance of grating-assisted output couplers. Grating structures have been studied extensively [1, 2] for their use in microwave, millimeter-wave, and optical devices and systems. A number of methods, both analytical and numerical, have been proposed to analyze these grating structures for single-frequency excitation. Most of them treat the gratings as periodic structures of infinite extent with reasonably homogeneous, nondispersive materials in each unit cell. However, for ultrafast pulse applications, finite, aperiodic gratings are necessary to achieve efficient performance. Complex material properties must also be taken into account. Few modeling approaches can handle finite, aperiodic structures in complex material environments.

The finite-difference time-domain method (FDTD) [3] is a very good choice for this purpose. First introduced by Yee [4], this discrete numerical method directly solves the full-wave vector Maxwell's equations in differential form. It has become a very popular method, and has been successfully applied to a variety of electromagnetic problems [5]. Recently, FDTD simulations have been shown to be very effective in modeling complicated grating structures [6, 7]. It provides an extremely flexible simulation environment that can model arbitrary geometries and material distributions, including dispersion and nonlinearities.

We will examine, in the presence of dispersive materials, grating-assisted couplers designed to convert pulsed incident guided modes into radiated modes at certain predefined angles. Specifically, we will examine the effects of dispersion on the resulting far-field patterns. These patterns are obtained with a near-field to far-field transform capability [8] incorporated into the FDTD simulator. Moreover, we will examine different approaches used in the FDTD method to model Lorentz material dispersion. We then will study two configurations of the grating-assisted output couplers excited by ultrafast pulsed modes in which either the basis waveguide or the grating teeth are composed of dispersive materials.

2. LORENTZ DISPERSION

We will use the Lorentz dispersion model to describe the dispersion effects. This type of dispersion is frequently encountered; it exhibits a rapid variation in the resulting propagation and absorption properties of the dielectric around its resonance frequency. Lorentz dispersion is described in the frequency domain by the following expression for the dielectric permittivity (the engineering $e^{j\omega t}$ time convention is assumed):

$$\epsilon_r(\omega) = \epsilon_\infty + \frac{(\epsilon_s - \epsilon_\infty)\omega_0^2}{\omega_0^2 + 2j\omega\delta - \omega^2} \tag{1}$$

where ω_0 is the resonance frequency, δ is the damping constant (the half-width at half-maximum of the absorption coefficient versus frequency), and ϵ_s and ϵ_∞ are, respectively, the dielectric constant at dc and infinite frequency. Figure 1 shows the real and imaginary parts of the dielectric permittivity when $\epsilon_s = 2.67$, $\epsilon_\infty = 1.0$, $\omega_0 = 12.94 \times 10^{14}$ rad/s, and $\delta = 10^{13}\text{s}^{-1}$.

With Lorentz dispersion, both the real part and imaginary parts of the dielectric permittivity undergo rapid variations near the resonance frequency. The region in which the derivative with respect to frequency is negative (positive) is the anomalous (regular) dispersion region. We observe that anomalous dispersion occurs in a frequency band centered at the resonance frequency. In addition, strong absorption occurs in the anomalous dispersion region. The latter is one of the major reasons that we only used the regular dispersion region for the following investigation.

Lorentz dispersion can also be described in the time domain by the polarization vector $\mathbf{P}(\mathbf{r}, t)$. Lorentz material dispersion is characterized in the time domain as a damped harmonic oscillator according to the ordinary differential equation

$$\frac{\partial^2}{\partial t^2}\mathbf{P}(\mathbf{r}, t) + \Gamma\frac{\partial}{\partial t}\mathbf{P}(\mathbf{r}, t) + \omega_0^2\mathbf{P}(\mathbf{r}, t) = \epsilon_0\chi\omega_0^2\mathbf{E}(\mathbf{r}, t) \tag{2}$$

where ω_0 and Γ are, respectively, the resonance frequency and the damping coefficent (full-width at half-max of the absorption coefficient versus frequency). This time-domain form of the Lorentz material dispersion model must be incorporated into the FDTD simulator to model the dispersion effects. It can be shown that the frequency domain (1) and time domain (2) representations are equivalent, provided that $\Gamma = 2\delta$ and $\chi = \epsilon_s - 1$.

3. FDTD DISPERSION FORMULATIONS

The representations expressed in Eqs. (1) and (2) lead to two different FDTD dispersion formulations: the auxiliary differential equation (ADE) approach [19, 10], and the polarization equation (PE) approach [11, 12]. These methods both introduce additional ordinary differential equations to be solved self-consistently with the original Maxwell's equations. We note that both approaches can be used for modeling nonlinearities as well as dispersion.

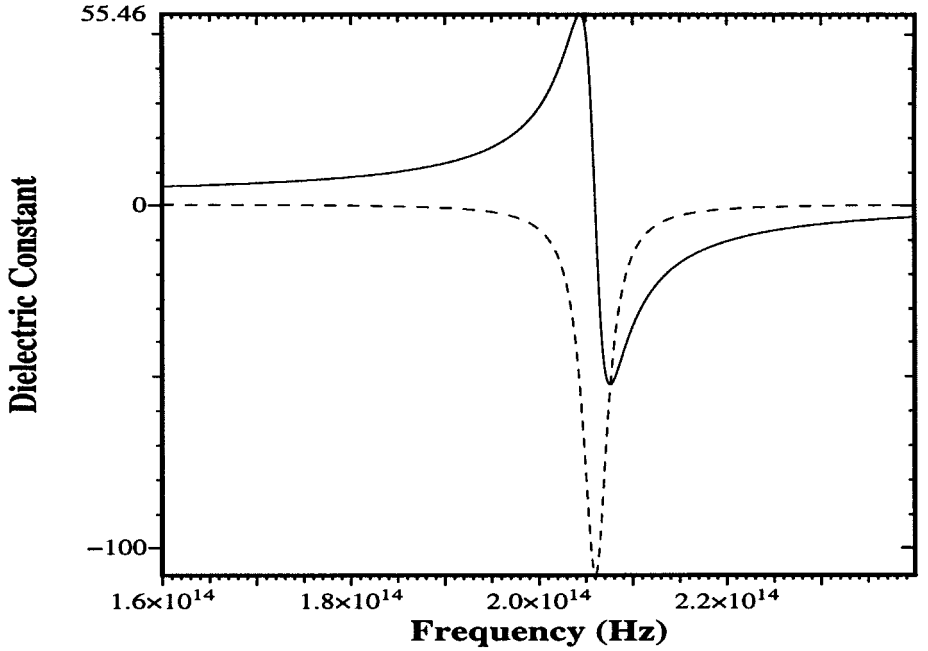

Figure 1 Lorentz dispersion. The real part (solid line) and the imaginary part (dotted line) of the dielectric permittivity are shown as functions of frequency

For the ADE approach, a second-order time-domain differential equation relating $\mathbf{D}(\mathbf{r}, t)$ and $\mathbf{E}(\mathbf{r}, t)$ is introduced to augment Maxwell's equations. It is based on the assumption that the electric susceptibility can be written in a rational form as a function of the angular frequency. In contrast to the usual update equation for $\mathbf{E}(\mathbf{r}, t)$, one introduces a field update equation for the electric flux density $\mathbf{D}(\mathbf{r}, t)$. The differential equation relating $\mathbf{D}(\mathbf{r}, t)$ and $\mathbf{E}(\mathbf{r}, t)$ is then used to find the updated value of $\mathbf{E}(\mathbf{r}, t)$. This value of $\mathbf{E}(\mathbf{r}, t)$ is then used in the standard FDTD update equation for the magnetic field $\mathbf{H}(\mathbf{r}, t)$. This approach requires a back store for one previous time step for $\mathbf{D}(\mathbf{r}, t)$ and $\mathbf{E}(\mathbf{r}, t)$ to achieve the corresponding FDTD updates. For the specific details of the FDTD implementation of the Lorentz dispersion model with the ADE approach, see [3].

For the PE approach, the polarization vector $\mathbf{P}(\mathbf{r}, t)$ is introduced instead of the electric flux vector $\mathbf{D}(\mathbf{r}, t)$. Direct treatment of the polarization vector $\mathbf{P}(\mathbf{r}, t)$ is advantageous because it is the source of the material properties. There have been many other models developed to describe material properties that can be treated in a similar fashion. The PE approach requires the introduction of the polarization current $\mathbf{J}(\mathbf{r}, t)$:

$$\mathbf{J}(\mathbf{r}, t) = -\frac{\partial}{\partial t}\mathbf{P}(\mathbf{r}, t). \tag{3}$$

The polarization field relation (2) then yields an equation for this polarization current:

$$\frac{\partial}{\partial t}\mathbf{J}(\mathbf{r}, t) + \Gamma\mathbf{J}(\mathbf{r}, t) = \omega_0^2(\epsilon_0 \chi \mathbf{E}(\mathbf{r}, t) - \mathbf{P}(\mathbf{r}, t)). \tag{4}$$

Equations (3) and (4) are then solved with Maxwell's equations in a self-consistent, explicit manner as a first-order system of differential equations.

We concentrated our study on the two-dimensional TE polarization case in which the field components H_x, E_y, and H_z exist. The propagation direction in the dielectric waveguide is along the z-axis. For the implementation of Lorentz dispersion with the PE approach in our FDTD simulator, we further introduce the unknowns P_y and J_y, and assign them at the same spatial locations (cell centers) as E_y, and update E_y and P_y at integer time steps and J_y at half-integer time steps, respectively. Using Standard central differencing notation, we obtain the following update equations:

$$\begin{aligned} E_y^{n+1}(i,k) = E_y^n(i,k) &- \frac{\Delta t}{\epsilon_0} J_y^{n+\frac{1}{2}}(i,k) \\ &+ \frac{\Delta t}{\epsilon_0 \Delta z}\left[H_x^{n+\frac{1}{2}}(i,k+1) - H_x^{n+\frac{1}{2}}(i,k)\right] \\ &- \frac{\Delta t}{\epsilon_0 \Delta x}\left[H_z^{n+\frac{1}{2}}(i+1,k) - H_z^{n+\frac{1}{2}}(i,k)\right] \end{aligned} \tag{5}$$

$$P_y^{n+1}(i,k) = P_y^n(i,k) + \Delta t J_y^{n+\frac{1}{2}}(i,k) \tag{6}$$

$$\begin{aligned} J_y^{n+\frac{3}{2}}(i,k) = &\frac{1 - \frac{\Gamma\Delta t}{2}}{1 + \frac{\Gamma\Delta t}{2}} J_y^{n+\frac{1}{2}}(i,k) \\ &- \frac{\omega_0^2 \Delta t}{1 + \frac{\Gamma\Delta t}{2}} p_y^{n+1}(i,k) \\ &+ \frac{\omega_0^2 \Delta t \epsilon_0 \chi}{1 + \frac{\Gamma\Delta t}{2}} E_y^{n+1}(i,k) \end{aligned} \tag{7}$$

The update equations for H_x and H_z have their standard forms [3].

4. NUMERICAL RESULTS AND ANALYSIS

We investigated the effects of dispersion for the two grating/waveguide combinations shown in Figure 2. Lorentz dispersion is incorporated into the slab waveguide in the first case and into the grating teeth in the second case. The dispersive slab waveguide extends for five grating cells with five perfect electric conducting (PEC) teeth imposed on the upper side of it. For the second case, there are 11 dispersive dielectric grating teeth. The grating period Λ for both cases is 1.12 μm, which is selected to scatter an incident, single-frequency guided wave at a carrier frequency of 2×10^{14} Hz into the direction normal to the waveguide. The PEC gratings and dielectric gratings have a duty factor of 0.5 and depths of 0.2 and 0.4 μm, respectively. The deeper dielectric grating tooth depth is used compared to the PEC grating in order to increase the effect of dispersion for the penetrable grating tooth case.

The dielectric waveguide is excited [6] through a total field/scattered field source which excites a pulsed fundamental mode that consists of the spatial fundamental mode of the

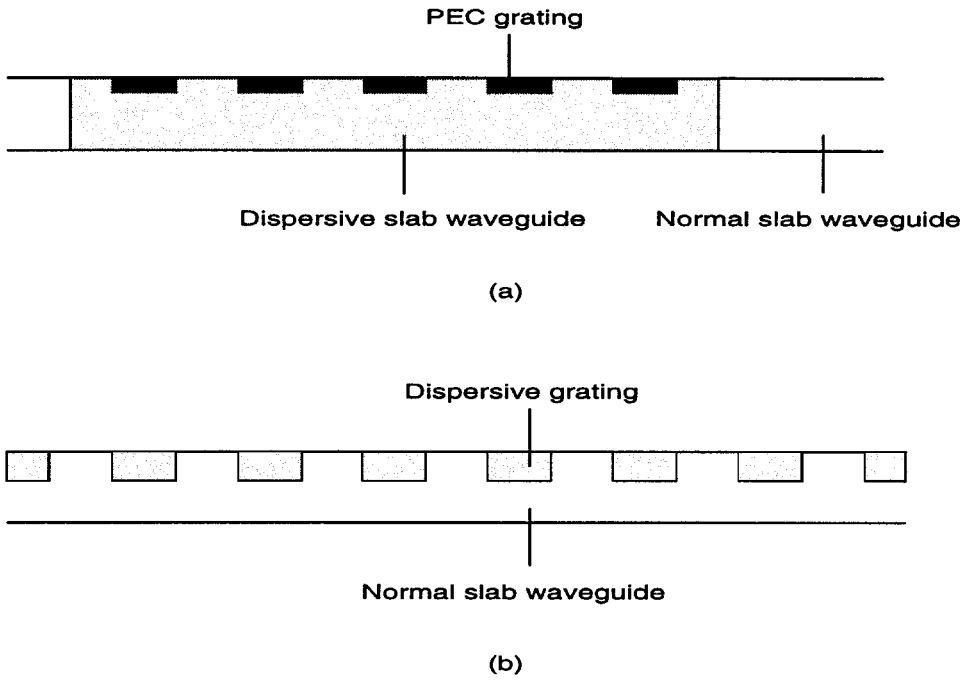

Figure 2 Grating-assisted output couplers problem geometries used for investigating dispersive effects for (a) a dispersive slab waveguide with PEC grating teeth, and (b) a nondispersive slab waveguide with dispersive dielectric grating teeth

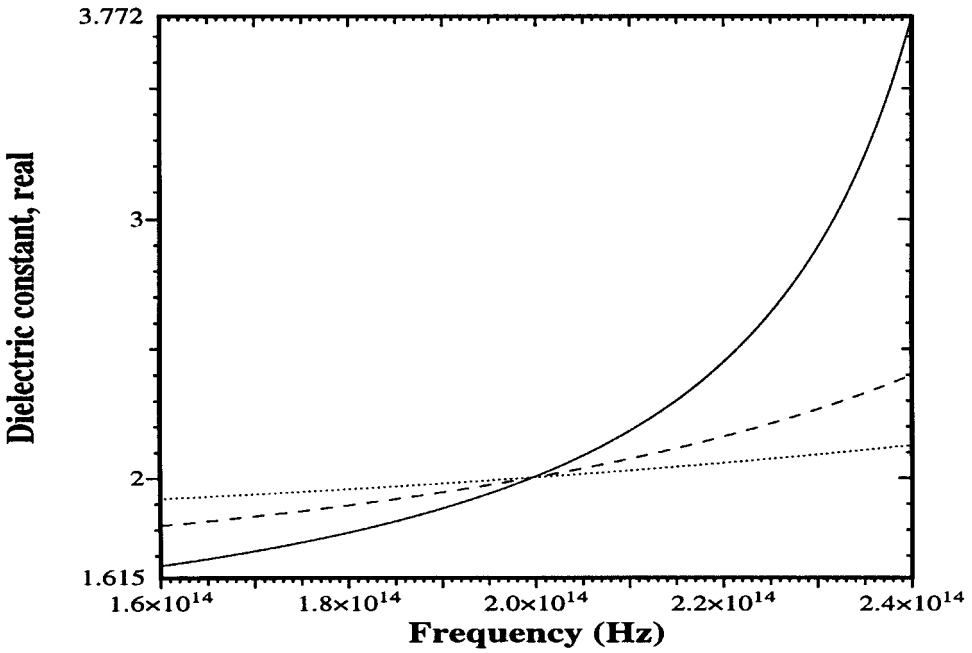

Figure 3 Dispersion properties of the slab waveguide. The resonance frequencies of the associated Lorentz dispersion model were taken to be $1.3\omega_c$ (solid line), $1.6\omega_c$ (dashed line), and $2.2\omega_c$ (dotted line)

waveguide multiplied by a time signal. The time signal is an N–M–N pulse constructed from a sinusoidal time history having carrier frequency ω_c and a window function which is constructed from a smooth turn-on from 0 to 1 over N cycles, a unit amplitude for M cycles, and a smooth turn-on from 1 to 0 over N cycles. The simulations below were initiated with a 2–2–2 pulsed fundamental mode having a carrier frequency of $\omega_c = 2\pi f_c$, where $f_c = 2 \times 10^{14}$ Hz.

The dispersion is varied by adjusting the resonance frequency ω_0 relative to the carrier frequency ω_c. The closer the carrier frequency is to the resonance frequency, the larger the dispersive effects will be. The dispersion parameters are selected to have small absorption associated with the imaginary part of the dielectric permittivity. We used the values $\epsilon_\infty = 1.0$ and $\delta = 2.8 \times 10^7$ s^{-1}. Once the resonance frequency was chosen, the value of ϵ_s was then calculated in order to have the desired dielectric constant at the carrier frequency. For the dispersive slab waveguide, the dielectric constant at the carrier frequency is set to be 2.0. Figure 3 shows the real part of the dielectric constant for three cases

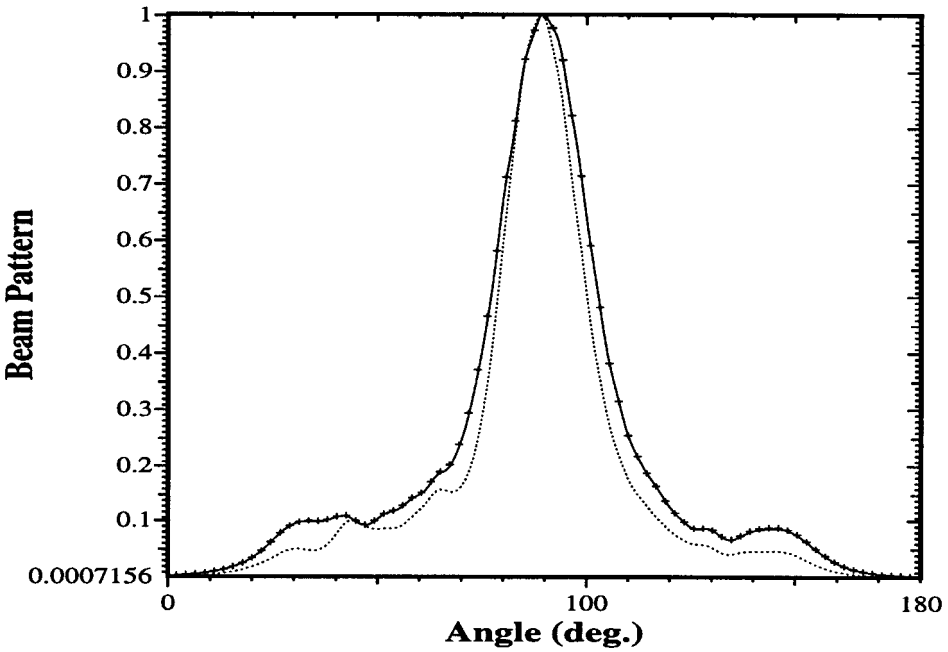

Figure 4 Comparison between the beam patterns generated with the PE (solid line) and ADE (marker) dispersion formulations. Shown in the dotted line is the pattern obtained with the corresponding nondispersive slab waveguide

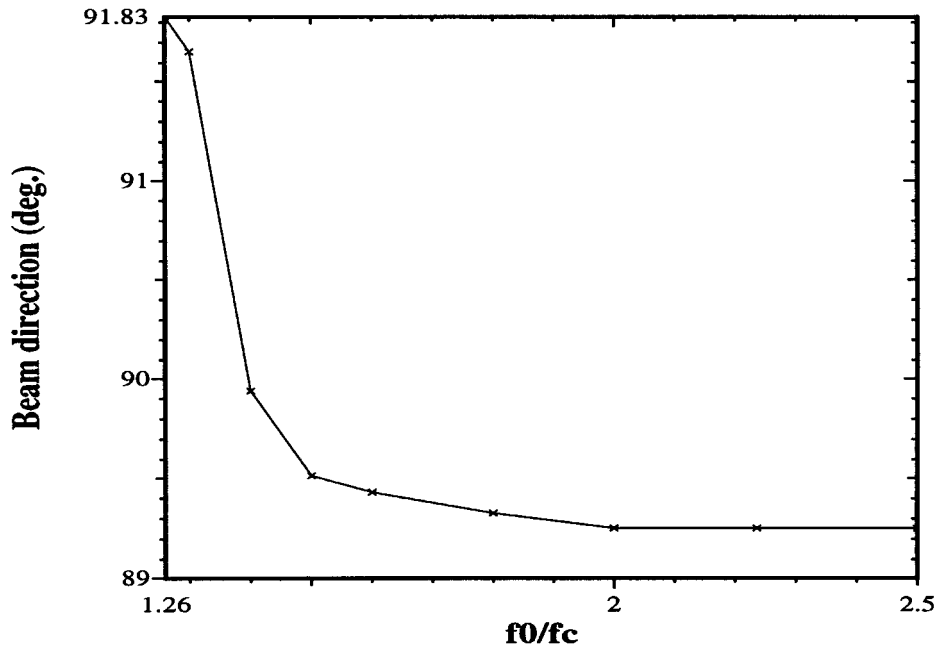

Figure 5 Effect of dispersion on the direction of the maximum output from the grating-assisted output coupler as a function of the frequency ratio f_0/f_c

where the resonance frequencies of the associated Lorentz dispersion in the slab waveguide are, respectively, 1.3 (solid line), 1.6 (dashed line), and 2.2 (dotted line) times the carrier angular frequency ω_c.

We first compare the two FDTD Lorentz dispersion model implementations described above. The far-field pattern for the grating-assisted output coupler consisting of five PEC grating teeth imposed on the upper side of a dispersive slab waveguide having $\omega_0 = 1.3\omega_c$ was computed with both the PE formulation and the ADE formulation. The results of these simulations are presented in Figure 4; they show that the two formulations produce equivalent values. Nonetheless, we note that the PE formulation, when compared algorithmically to the ADE formulation, retains more of the physical meaning of the polarization model, does not need any backstores of data, and is more straightforward to implement.

Also shown in Figure 4 is the far-field pattern obtained with the slab waveguide being nondispersive. One can see immediately that the dispersion causes a variation in the output direction, an increase in the beam width, and more distortion in the far-field pattern. To further quantify the effects of dispersion on the far-field pattern, we measured the

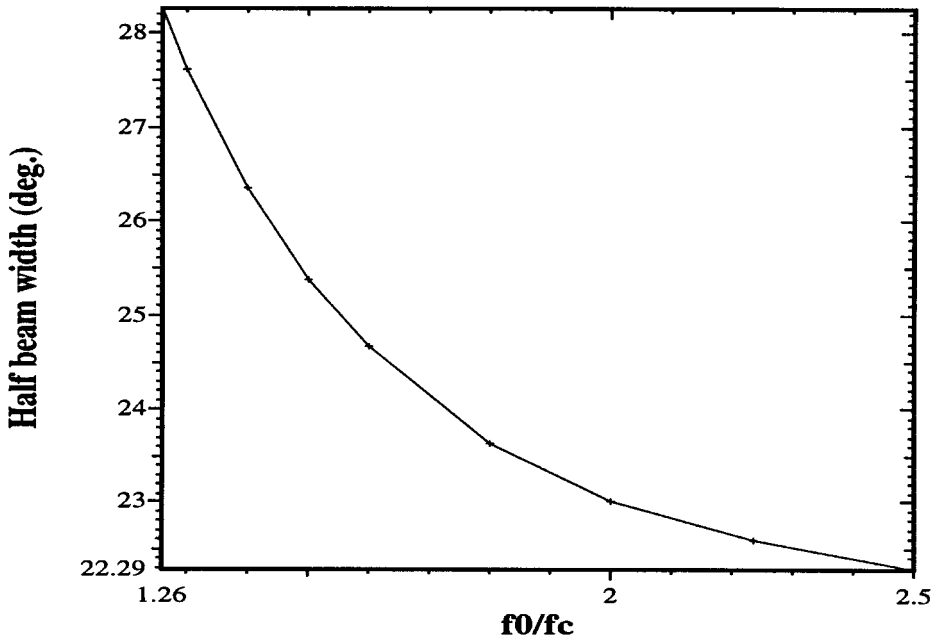

Figure 6 Effect of dispersion on the half beam width of the grating-assisted output coupler's far-field pattern as a function of the frequency ratio f_0/f_c

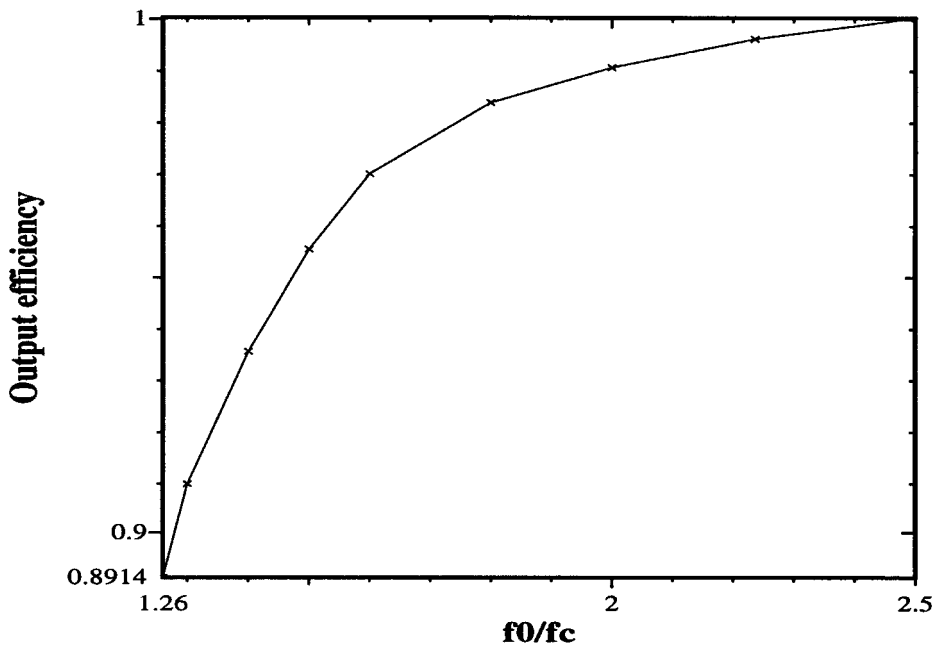

Figure 7 Effect of dispersion on the output efficiency of the grating-assisted output coupler as a function of the frequency ratio $f0/fc$

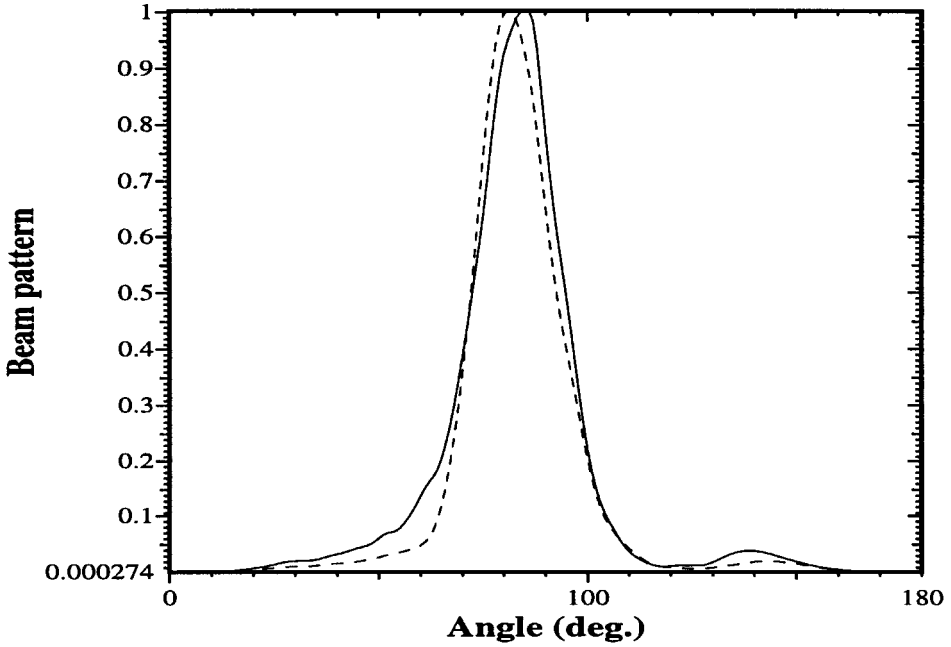

Figure 8 Far-field patterns obtained with a dielectric grating-assisted output coupler having dispersive (solid line) and nondispersive (dashed line) teeth

maximum beam direction, the half beam width, and the output coupling efficiency as the dispersion parameters varied. These results are presented in Figures 5–7 respectively. We see a shift of the beam direction, a widening of the half beam angle, and a reduced coupling efficiency as the dispersion becomes more pronounced, i.e., for resonance frequencies closer to the carrier frequency. This shift is a direct result of the change due to the dispersion in the index of refraction which directly impacts the phase-matching condition.

We also examined the effects of dispersion associated with the dispersive dielectric grating teeth as depicted in Figure 2(b). For this case, dielectric grating teeth with Lorentz dispersion are imposed on a nondispersive slab waveguide. The dispersive grating teeth have a dielectric constant of 4.0 at the carrier frequency; the slab waveguide has a dielectric constant of 2.0. Similar impacts on the far-field patters were observed. Figure 8 shows the far-field pattern obtained from a grating-assisted output coupler consists of 11 dispersive dielectric grating teeth with the resonance frequency of the Lorentz dispersion being set to $\omega_0 = 1.35\omega_c$. The pattern obtained with the corresponding output coupler with nondispersive dielectric teeth having a dielectric constant of 4.0 is included as the dashed line for comparison. The effects of dispersion resulting from the presence of dispersion in the teeth of the grating are now easily recognizable. We note that these effects are smaller compared to the case when the coupler consisting of the PEC grating teeth and a dispersive slab waveguide. This is caused by the reduced size of the dispersive region and radiation output coupling efficiency of the dielectric grating.

5. CONCLUSIONS

In conclusion, the FDTD method is an effective simulation tool for characterizing structures in the presence of complex material properties, including dispersion effects. The material properties are assigned to each Yee cell, and the boundary conditions are enforced at all material interfaces. It is thus a general and robust method. We examined two dispersion formulations, the PE and ADE methods, that can be used in FDTD simulators, and found that they produce equivalent results. We further studied the impact of dispersion on the performance of grating-assisted output couplers. We quantified the variations in the far-field patterns generated from grating-assisted output couplers due to the effects of dispersion in the material present in the couplers. The dispersion parameters used in the FDTD simulations were relatively weak because we purposely chose to work in the regular dispersion regime away from the resonance frequency of the Lorentz dispersion model, where the absorption effects would become significant and the output coupling would have been substantially reduced. We found that material dispersion causes a variation in the output beam direction, a widened output beam width, a reduced output coupling efficiency. Dispersion was also found to cause the sidelobe levels in the far-field patterns to increase. This investigation strongly suggests that the material dispersion properties of any grating-assisted output coupler should be taken into consideration when excited with an ultrafast pulse since these pulses possess very wide spectral contents.

ACKNOWLEDGMENTS

This effort was sponsored in part by the Office of Naval Research under Grant N0014-95-1-0636 and by the Air Force Office of Scientific Research, Air Force Materials Command, USAF, under Grant F49620-96-1-0039.

REFERENCES

1. R. Petit, *Electromagnetic Theory of Gratings*, Springer-Verlag, New York, 1980.
2. D. Marcuse, *Theory of Dielectric Optical Waveguides*, Academic Press, New York, 1991.
3. A. Taflove, *Computational Electrodynamics*, Artech House, Norwood, MA, 1995.

4. K. S. Yee, "Numerical Solution of Initial Boundary Value Problems Involving Maxwell's Equations in Isotropic Media," *IEEE Trans. Antennas Propagat.*, Vol. 44, 1996, pp. 302–307.
5. K. L. Shlager and J. B. Schneider, "A Selective Survey of the Finite-Difference Time-Domain Literature," *IEEE Antennas Propagat. Mag.*, Vol. 37, No. 4, 1995.
6. T. Liang and R. W. Ziolkowski, "Mode Conversion of Ultrafast Pulses by Grating Structures in Layered Dielectric Waveguides," *J. Lightwave Technol.*, Sept. 1997.
7. R. W. Ziolkowski and T. Liang, "Design and Characterization of a Grating-Assisted Coupler Enhanced by a Phototonic-Band-Gap Structure for Effective Wavelength-Division Demultiplexing," *Opt. Lett.*, July 1997, pp. 1033–1035.
8. K. Kunz and R. Lubbers, *The Finite Difference Time Domain Method for Electromagnetics*, CRC Press, Boca Raton, FL, 1993.
9. T. Kashiwa and I. Fukai, "A Treatment by FDTD Method of Dispersive Characteristics Associated with Orientation Polarization," *Trans. Inst. Electron. Inf. Commun. Eng.*, Vol. 73, 1990, pp. 1326–1328.
10. R. M. Joseph, S. C. Hagness, and A. Taflove, "Direct Time Integration of Maxwell's Equations in Linear Dispersive Media with Absorption for Scattering and Propagation of Femtosecond Electromagnetic Pulses," *Opt. Lett.*, Vol. 16, 1991, pp. 1412–1414.
11. R. W. Ziolkowski, "The Incorporation of Microscopic Material Models into the FDTD Approach for Ultrafast Optical Pulse Simulations," *IEEE Trans. Antennas Propagat.*, Vol. 45, 1997, pp. 375–391.
12. R. W. Ziolkowski, "The Design of Maxwellian Absorbers for Numerical Boundary Conditions and for Practical Applications Using Engineered Artificial Materials," *IEEE Trans. Antennas Propagat.*, Vol. 45, 1997, pp. 656–671.

CCC 0895-2477/98

HIGH-POWER TERAHERTZ RADIATION FROM A HIGH-REPETITION-RATE LARGE-APERTURE PHOTOCONDUCTING ANTENNA

G. Mouret,[1] W. Chen,[1] D. Boucher,[1] R. Bocquet,[2] P. Mounaix,[3] D. Théron,[3] and D. Lippens[3]
[1] Laboratoire de Physico – Chimie de l'Atmosphère
Université du Littoral
59140 Dunkerque, France
[2] Laboratoire de Spectroscopie Hertzienne
Université des Sciences et Technologies de Lille
59655 Villeneuve d'Ascq Cedex, France
[3] Institut d'Electronique et de Microélectronique du Nord
B.P. 69, 59652 Villeneuve d'Ascq Cedex, France

Received 23 July 1997

ABSTRACT: *While the majority of research with terahertz radiation from large-aperture antennas used high-intensity femtosecond laser pulses with low repetition rates, we used a regenerative amplifier with a repetition rate up to 300 kHz. This high repetition rate allows us to combine a high-power large-aperture transmitter and dipole antenna detection.* © *1998 John Wiley & Sons, Inc.* Microwave Opt Technol Lett 17: 23–27, 1998.

Key words: *terahertz radiation; photoconducting antenna; LTG–GaAs; femtosecond techniques*

INTRODUCTION

Pulsed electromagnetic radiation with terahertz bandwidth but relatively limited power has been produced in the past by means of femtosecond optical pulses incident upon Hertzian dipoles, strip lines, and spiral antennas [1]. Various applications include time-domain spectroscopy of liquids [2], gas [3], semiconductors [4], superconductors [5], flames [6], and organic samples [7]. In this study, we use a low-intensity femtosecond laser (few nanojoules per pulse) with a high repetition rate ($\approx$ 100 MHz).

For other applications such as saturation phenomena and nonlinear processes in semiconductors, a high peak power is required [8, 9]. This motivates the development of a large-aperture antenna which accepts high optical fluence and high applied voltage. You et. al. have produced high-peak-power terahertz radiation (1.5 MW) with a Ti:Sa chirped-pulse amplifier system which operates at a repetition rate of 10 Hz from a 3-cm large-aperture transmitter [10].

The detection scheme depends on the terahertz transmitter. In low-power experiments, the same system is generally used for the detector. The switch is biased by the incoming terahertz radiation pulse. On the other hand, the measurement is carried out by shortening the detector gap by means of femtosecond optical pulses, and by measured the collected charge versus the time delay between the pump and probe signals. the Fourier transform of the temporal shape of the detected current reflects the spectrum of the radiating field. Both amplitude and phase information is available, and hence the detection systems is a coherent process [11]. As a general rule, the repetition rate of the femtosecond laser is crucial for the signal-to-noise ratio. Indeed, the signal level increases linearly with the number of sampling pulses, while the noise increases only as the square root of the number of pulses [11].

Under these conditions, the low repetition rate of a high-power femtosecond laser can be troublesome for large-aperture transmitter experiments. One method to measure the spectral content of terahertz radiation employs a Michelson interferometer with a cooled bolometer. Another method uses a photoconductive switch as in the low-power terahertz experiments. This detector can operate at room temperature, but an operation at low repetition rate requires a large detection area, with the resulting bandwidth degradation [12, 13]. In addition, recent studies emphasize the importance of the repetition rate parameters with respect to intrinsic times of the physical processes involved [14]. Budiarto et al. [14] found that the output energy per pulse of the transmitter running at 1 kHz exceeded that at 100 Hz by as much as 60%, motivating a further increase in the repetition rate for this kind of experiment.

In this letter, we report an experiment which uses a high-repetition-rate system (up to 300 kHz) as an alternative approach for producing high-power electromagnetic pulses. For this purpose, we combine, for the first time to our knowledge, a large-aperture emitter antenna with a small-gap strip-line detector antenna. In addition, we have used nonstochiometric low-temperature-grown GaAs samples which offer great potential as extremely fast photoconducting detectors.

ANTENNA MATERIAL, STRUCTURE, AND FABRICATION

Low-temperature (LT)-grown GaAs epilayers were used for implementing the detecting antenna. Unlike GaAs materials grown at a substrate temperature of about 600°C, LT–GaAs contains a high concentration of deep defects which promote carrier recombination, but maintain good crystal quality. Optically generated carriers thus recombine at rates orders of magnitude larger than those grown at higher temperatures.